

## The Ion Source Development for Neutral Injection Heating at JAERI

H. Shirakata, T. Itoh, U. Kondoh,<sup>\*</sup> S. Matsuda, Y. Ohara, T. Ohga, T. Snibata,  
T. Sugawara,<sup>\*\*</sup> and S. Tanaka.

Japan Atomic Energy Research Institute

Tokai-mura, Ibaraki-ken, Japan

ABSTRACT: The neutral beam research and development effort at JAERI has been concentrated mainly on design, construction and testing of ion sources needed for the present and planned heating experiments. Fundamental characteristics of the ion sources developed are described.

### 1. INTRODUCTION

For the neutral beam research and development at JAERI, we built an ion source test stand ITS-1<sup>1)</sup> in Feb. 1975. Using this test stand we have developed and tested the ion source which will be used for the heating experiments on the JFT-2 tokamak. The basic characteristics of this source are discussed in Section 2. We are also investigating the geometrical scale up of the present system as a preliminary step for developing the injectors of JT-60. Since the final ion source for JT-60 may be a two stage accel system, these studies are necessary for the better understanding of the source plasma as well as of the first extraction stage of the two stage injectors. In particular, efforts are concentrated on beam optics, source plasma and cooling of the extraction electrodes which appears to be the basic problems involved in the high power and long duration ion source development.

\*\*\*\*\*

\*) On leave from Nissin Electric Co., Ltd.

\*\*\*) On leave from Research and Development Center, Tokyo Shibaura Ele. Co.

## 2. ION SOURCE FOR HEATING THE JFT-2 TOKAMAK PLASMA

Injection heating experiment using two beam lines is planned in the autumn of 1976. Composition of the equipment producing each beam line for JFT-2 tokamak is as follows; the window is of 56 mm x 120 mm, the drift tube reaches outside toroidal coils, and the neutralization cell of 8 cm diam. and 60 cm length is installed. The distance between the ion source and the window is 1.35 m. Each ion source can provide 6 A hydrogen ion beam at 30 kV. Since the ratio of this distance to the extraction electrode radius is comparable to the beam divergence angle, the transport efficiency is improved by focusing each beamlet from multi-apertures. Radial matching of the ion saturation current with the extraction current is also important for good optics of each beamlet. From this view point, the extraction gap is radially increased and the beamlet is focused by the aperture displacement method<sup>2,3)</sup>. The duoPIGatron<sup>4)</sup> is employed which has a set of accel-decel electrodes with 221 holes of 3.75 mm diam. each. The designed focal length is 1.4 m. The beam divergence of this electrode system is measured by a small movable calorimeter placed at 1.0 m apart from the source and is compared with that of the unfocused beam of 25 kV- 4.5 A from the disk electrodes. We find that the e-folding divergence angle is reduced from  $3.3^\circ$  to  $1.7^\circ$ .

The power supply of 30 kV- 30 A is designed to cope with the breakdown between accel-decel gaps. The accel voltage is regulated by the series tube, EIMAC Y-676 tetrode. The tube also serves to turn off the accel voltage in the case of breakdowns. The turn off time achieved at the test stand ITS-1 is less than 0.1 msec, and the tube is switched on after the breakdown is cleared. The decel power supply has a similar function.

Neutral beam composition has been measured with the neutralizer mentioned above. Momentum analysis of the beam passing through a slit of a front dumper, an electrostatic ion deflector, and a stripping cell is made by the

sweeping magnet. Figure 1 shows the power partition of charge-exchanged and dissociated neutral hydrogen beams in 30 kV extraction. The gas efficiency obtained is 57 %, which is defined by the ratio of accelerated hydrogen nuclei to cold leakage hydrogen nuclei. Impurity ion content is measured without using the neutralizer because the charge exchange cross sections of impurities are uncertain. The dominant impurities are oxygen and their hydride in our source. Their levels are high, especially, just after the installation of the new oxide filament. However, the steady state of low impurity level is attained after several hours of conditioning. Ultimately the amount of  $O^+$ ,  $OH^+$ ,  $H_2O^+$ , and  $H_3O^+$  are about 0.4 %, 0.4 %, 1.3 %, and 0.1 % of the total ion current, respectively.

Nearly constant gas flow is obtained by the pulsed feed system illustrated in Fig. 2. The gas flow rate is controlled by adjusting the reservoir pressure and the opening of the variable leak valve. The rise time of the gas flow is nearly equal to that of the solenoid valve.

### 3. GENERAL TOPICS

#### 3.1 Source Plasma Study

The spatial profiles of source plasma parameters are studied in 10 cm duoPIGatron. Typical ion saturation current density profiles measured by a Langmuire probe are shown in Figs. 3a and 3b. It is to be noted that the density decrease accompanying beam extraction is small even for large extraction of 7.9 A and that there is a significant axial decay of the density toward the target cathode which cannot be explained by the spread of magnetic lines of force. The electron temperature is about 10 eV and tends to be two components. The space potential is quite close to the anode potential even near the target cathode.

The typical drain current of this source is 8-9 A at 25-27 kV out of

which about 7.3 A are injected into the 20 cm diam. target placed 1.5 m apart from the extraction electrodes.

In order to obtain a more uniform plasma, the hollow feed methodes of source electrons are tested; namely, electrostatic repulsion by the button below the zwischen<sup>5,6)</sup>, the superposition of the dipole magnetic field by a loop current in the arc chamber, and the coaxial zwischen by inserting a magnetic pole at the axis. The structure of the coaxial zwischen is shown in Fig. 4. In this geometry the source plasma uniformity is extremely good and is within  $\pm 1\%$  over the 10 cm diam. target cathode.

### 3.2 Small Aperture Extractor

For the target cathode of the fixed area and transparency, a higher extraction current can be expected by employing smaller apertures on the basis of the scaling law of the beam extraction.<sup>7)</sup> In order to confirm the scaling, two sets of electrodes are tested. Their diameter is 7 cm each. The model-1 has 221 holes of 3.75 mm diam. each, and the model-11 693 holes of 2.2 mm diam. each. The results are shown in Fig. 5, where the equivalent beamlet divergence and the fraction of the beam power impinging on the grounded electrode are plotted against the perveance per hole. We are interested in the optimum perveance value  $P_c$ , where the divergence becomes minimum. In the model-1 electrode,  $P_c$  is about 5 micro-perves and is insensitive to the aspect ratio. Unlike our expectation,  $P_c$  in the model-11 electrode is too small, around 1 micro-perves for the decel gap  $z_d = 2$  mm. We suspect that the decel gap has a comparable importance with the accel gap. If we reduce the decel gap in keeping the aspect ratio constant, we find that  $P_c$  increases significantly. Although there still remains a difference by a factor of 2, it may be due to the unscaled electrodes thickness.

### 3.3 Beamlet Optics

Beamlet characteristics have been measured with the help of the Faraday Cup. Several geometries of the single aperture are tested. We find that

cutting the corner of the aperture in the positive electrode is effective in reducing the beam divergence. The e-folding divergence of the beam is shown in Fig.6. Here the minimum divergence is reduced to  $1.1^\circ$ , if one takes into account the deformation from the Gaussian distribution. A computer simulation code has been developed for the design of two stage accel system. In this model, the beam emitter surface is determined selfconsistently in such a way that the ion saturation current density is equal to that of the space charge limited current. No ions are emitted from the peripheral region of the boundary whose width corresponds to the thickness of the wall sheath  $\lambda$ . Figure 7 shows one of the computed examples for the proton beam. In order to investigate the validity of this code, computed beam divergence for the same geometry is compared with the experimental data (see Fig. 6). We find that the presence of the wall sheath is important for a reasonable agreement with the experiment.

#### 3.4 Cooling of Electrodes

For longer duration of the beam pulse, we have tested a set of copper electrodes with 16 parallel cooling water lines on the 10 cm diam. surface. Arrays of apertures and cooling pipes are arranged alternatively as shown in Fig. 8. Each aperture is 3.75 mm in diam. and the total number is 284, giving a transparency of 40 %. A time response of the temperature rise in the grounded electrode, where the heat load is the most serious, is measured with the 0.1 mm diam. Chromel-Alumel thermocouple buried in the center of the electrode. The beam current can be extracted up to 5 A at 30 kV for 0.5 sec. Due to the power supply capability, the drain current is limited to 1.3 A at 30 kV for the duration time exceeding 10 sec. However, owing to the improved beam optics the power loading on the grounded electrode stays nearly constant in our experimental current range. The temperature rises to saturate in about 3 sec after the initiation of the beam. The saturation of the temperature rise is attained at about  $150^\circ\text{C}$  which corresponds reasonably

well to the nucleate boiling point. By the detailed analysis of the rising phase, the temperature difference between the center of the bridge and the cooling pipe is obtained to be  $10^{\circ}\text{C}$ . This value is much lower than the allowable temperature difference of about  $40^{\circ}\text{C}$  determined from the mechanical stress of the electrode. Thus one envisages that these electrodes can be operated at a level of 5 A, 30 kV. However, the conclusion should be postponed until beam optics subject to deformation or displacement of apertures is investigated.

#### ACKNOWLEDGMENTS

The authors wish to thank S. Mori for encouraging them throughout the work. One of the authors wishes to express his appreciation to O.B. Morgan and members of the Plasma Heating Department at Oak Ridge National Laboratory for useful suggestions in constructing the ITS-1 test stand.

#### REFERENCES

- 1) S. Matsuda et al; JAERI-M 6431 (1976), in Japanese.
- 2) L.D. Stewart et al; Rev. Sci. Instr. 46 (1975) 1193.
- 3) Y. Ohara et al; JAERI-M 6438 (1976), in Japanese.
- 4) R.C. Davis et al; ORNL-TM 4675 (1974).
- 5) W. L. Stirling et al; Proceedings of the Second Symposium on Ion Sources and Formation of Ion Beams, Berkeley, California, 22-25 Oct. 1974.
- 6) D.A. Aldcroft et al; CLM-P 414 (1975).
- 7) J.R. Coupland et al; CLM-P 312 (1972).

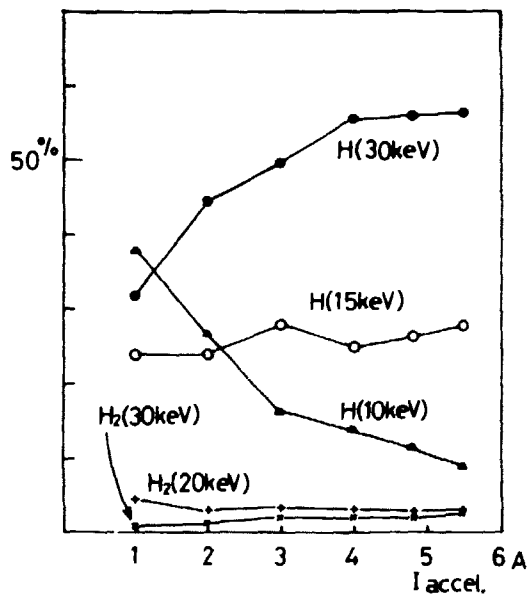
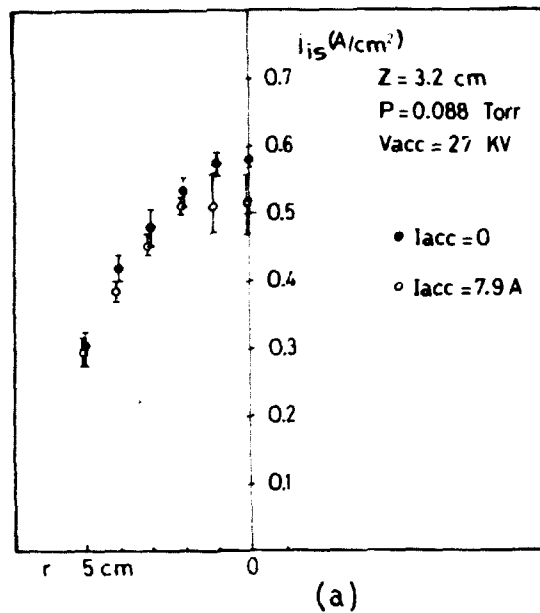


Fig. 1 Neutral power fractions at 30 kV extraction.



(a)

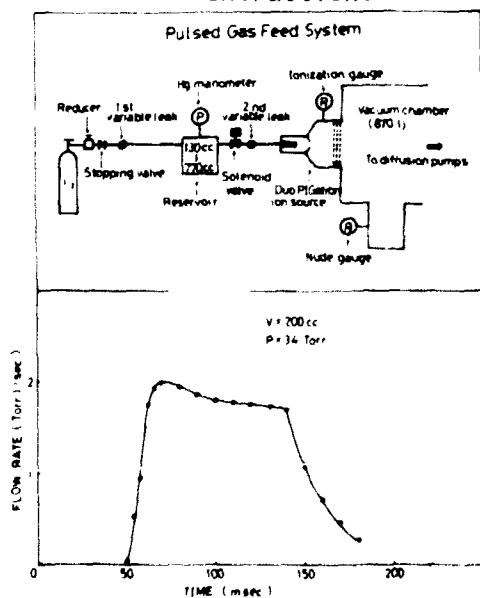
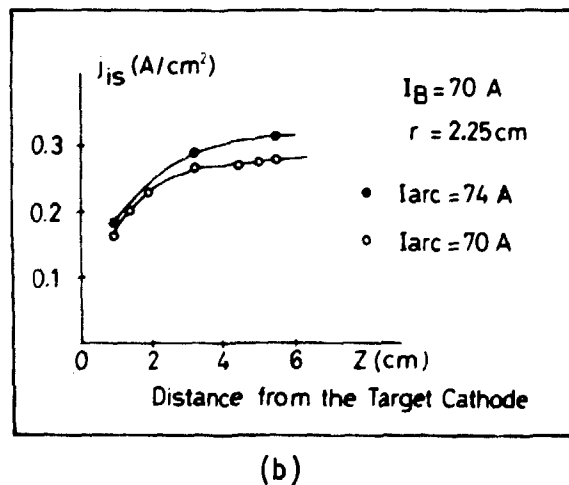


Fig. 2 Pulsed gas feed system and time behaviour of gas flow rates.



(b)

Fig. 3 (a) Radial profile of the ion saturation current in the beam on and off cases at  $z = 3.2$  cm. (b) Axial profile at  $r = 2.25$  cm in the beam off case.

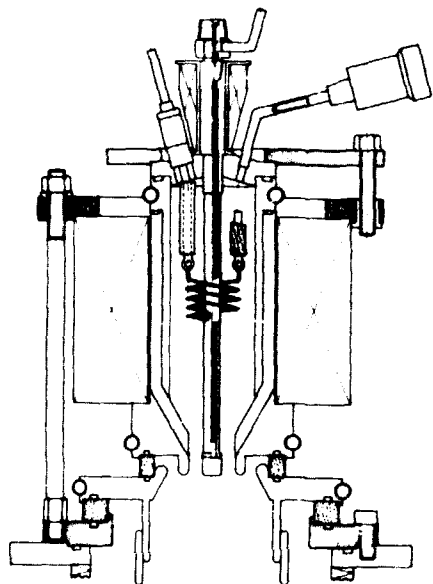


Fig. 4 Cross sectional view of the beam optics and power loading on the grounded electrode, where  $z_a$  and  $z_d$  are the accel and decel gaps, respectively.

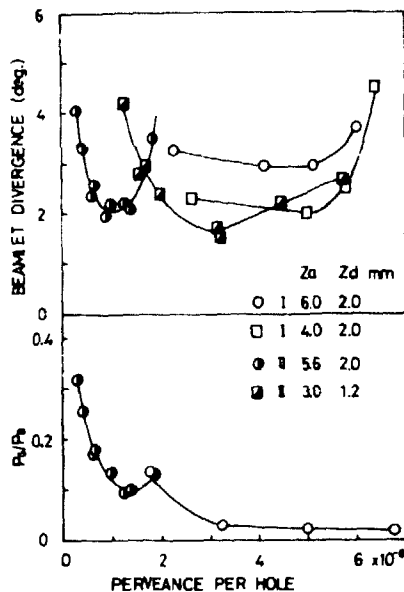


Fig. 5 Beamlet Divergence (deg) vs Perveance per Hole. Legend:  $z_a$   $z_d$  mm:  $\circ$  1.60 2.0,  $\square$  1.40 2.0,  $\bullet$  1.56 2.0,  $\blacksquare$  1.30 1.2.

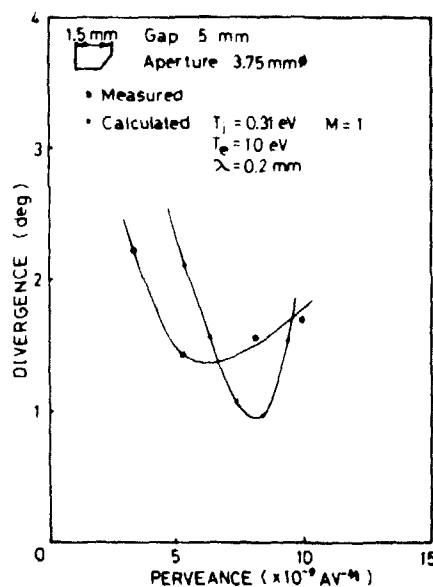


Fig. 6 Comparison of the measured beam divergence with calculated one.

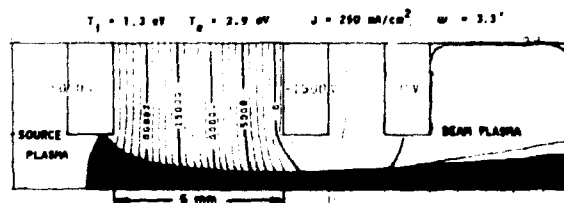


Fig. 7 Typical beam trajectories.  $T_i = 1.3 \text{ eV}$ ,  $T_e = 2.9 \text{ eV}$ ,  $J = 250 \text{ mA/cm}^2$ ,  $\omega_{pe} = 3.3^\circ$ .

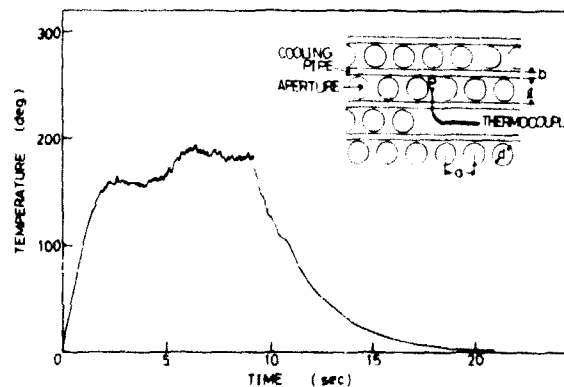


Fig. 8 Time behavior of the temperature rise at the center of the grounded electrode. Operating condition:  $V_{acc} = 30 \text{ kV}$ ,  $I_{acc} = 1.3 \text{ A}$ , total flow rate of cooling water; 2 l/min. Geometry of electrode:  $a = 4.44 \text{ mm}$ ,  $b = 1.2 \text{ mm}$ ,  $d = 3.75 \text{ mm}$ ,  $l = 4.9 \text{ mm}$ .